

A COMPREHENSIVE STUDY ON THE USE OF SUB-COHERENT SELF
HETERODYNE LINEWIDTH ESTIMATIONS

By

Genevieve Gutierrez

Bachelor of Science-Mechanical Engineering
Bachelor of Science-Applied Physics
University of Nevada, Las Vegas
2023

A thesis submitted in partial fulfillment
of the requirements for the
Master of Science - Physics

Department of Physics and Astronomy
College of Sciences
The Graduate College

University of Nevada, Las Vegas
August 2025



Thesis Approval

The Graduate College
The University of Nevada, Las Vegas

July 14th, 2025

This thesis prepared by

Genevieve Gutierrez

entitled

A Comprehensive Study on The Use of Sub-Coherent Self Heterodyne Linewidth
Estimations

is approved in partial fulfillment of the requirements for the degree of

Master of Science - Physics
Department of Physics and Astronomy

Yan Zhou, Ph.D.
Examination Committee Chair

Bernard Zygelman, Ph.D.
Examination Committee Member

Joshua Island, Ph.D.
Examination Committee Member

Jan Pedersen, Ph.D.
Graduate College Faculty Representative

Alyssa Crittenden, Ph.D.
*Vice Provost for Graduate Education &
Dean of the Graduate College*

Abstract

A fundamental requirement for many precision spectroscopic applications is the development of stable lasers with narrow linewidths. However, accurately verifying laser linewidths becomes increasingly challenging as the linewidth decreases. In the field of frequency metrology, the delayed self-heterodyne technique has long been regarded as one of the most reliable and accessible methods for linewidth characterization, favored for its low equipment cost and reproducible results. Traditionally, self-heterodyne measurements employ an optical delay line significantly longer than the coherence length of the laser, with analysis performed via either the instantaneous power spectral density or the noise power spectral density. However, the use of long optical fibers introduces several limitations: substantial optical attenuation requiring amplification stages, and susceptibility to thermally induced Brownian noise, which can artificially broaden the measured spectrum. This work utilizes a short delay fiber – less than the laser’s coherence length – can yield reliable and accurate linewidth measurements. The primary objective of this thesis is to provide a comprehensive methodology for extracting the laser linewidth from the power spectral density of a sub-coherence delay self-heterodyne signal, thereby offering an improved framework for precision laser characterization.

Acknowledgments

I wish to thank Dr Yan Zhou for the support and guidance he has provided me throughout the last 4 years in both undergraduate and graduate school. This project would not be possible with him. I would also like to thank my peer, Rodrigo Fernandez, as he was an exceptional lab mate. Without his help, the last two years would have been much more difficult.

Table of Contents

Abstract	iii
Acknowledgment	iv
List of Figures	vi
1 Introduction	1
2 Theory	3
2.1 Random Signal Analysis	5
2.2 Phase Noise and the Diode Lineshape	7
2.3 Beat note Generation and Linewidth Extraction	11
3 Experiments	17
3.1 Self-Heterodyne Design	17
3.2 ECDL Design	19
3.3 Fitting Procedure	23
3.4 Rb Spectroscopy	24
4 Results	27
4.1 Rb Locking and the ECDL Upper Bound	27
4.2 Noise Floor and Window Function Modeling	29
4.3 Linewidth and Delay Time	31
4.4 Spectrum Broadening Noise Sources	35
5 Conclusion	38
References	39
Curriculum Vitae	41

List of Figures

2.1	Fourier Transform and Power Spectral Density of a 100Hz Noisy Signal .	3
2.2	Energy Diagram of a Two Level System	4
2.3	(a) Fabry Perot Cavity, (b) Cavity Transmission, (C)Zoom in of a Trans- mission Peak	11
2.4	(a) Self Homodyne Technique, (b) Self Heterodyne Technique	14
3.1	AOM Diagram	17
3.2	Experimental Setup of Self heterodyne Experiment	19
3.3	Comparison of PSD Size for Different Linewidths	20
3.4	Plot of Extrema Difference as a Function of Linewidth	20
3.5	780 nm ECDL	21
3.6	(a) Example of PSD using 120 m Delay Length, (b) Zoom in of Delta Feature	23
3.7	Diagram of ^{87}Rb D-line Transitions	24
3.8	Saturated Absorption Scheme Used for Measuring ^{87}Rb Transitions . . .	25
3.9	Graphic of Derivative of Transition Discriminant Generation [1]	26
4.1	Experimentally Observed ^{87}Rb Transitions (Orange) and the FM Gener- ated Derivative (Blue)	28
4.2	(a) Zoom-in of Delta Feature, (b) Comparison of Delta Feature Response to Different Resolution Bandwidths (30 kHz in orange, 3 kHz in blue, (c) Fitting of the Delta Feature to a Gaussian of Width Equal to RBW . . .	28
4.3	Comparison of Extracted Delta Feature Width and Set RBW	30
4.4	(a)Comparison of Noise Level for a Single Scan at 10 kHz RBW (Blue), and Average of 16 Measurements (Orange), (b)Residual of Average and Single Scan	31
4.5	(a)PSD of the 780 nm ECDL using a 120 m Delay Fiber,(b)PSD of the 780 nm ECDL using a 2000 m Delay Fiber	32

4.6	(a) ^{87}Rb Spectrum with large modulation depth, (b)PSD of 780 nm ECDL with large Modulation Depth, (c) ^{87}Rb Spectrum with small modulation depth, (d)PSD of 780 nm ECDL with Small Modulation Depth	33
4.7	(a)950 nm DFB PSD with 120 m Delay, (b)950 nm DFB PSD with 2000 m Delay, (c)720 nm DL Pro PSD with 120 m Delay, (d)720 nm DL Pro PSD with 2000 m Delay	34
4.8	(a)Fit to 780 nm PSD using a Correction for 1/f Noise in 120 m Fiber, (b)Fit to 780 nm PSD using a Correction for 1/f Noise in 2000 m Fiber .	36
4.9	Current Induced 1/f Noise in 950 nm DFB	37

1 Introduction

Over the past several decades, there has been a continuous push to interrogate atomic, molecular, and subatomic systems with increasingly higher levels of precision. As scientists have pursued ever more accurate spectroscopic measurements, laser technology has evolved in parallel to meet these stringent demands. Among the critical laser characteristics that have come under intense focus is coherence time, which plays a fundamental role in determining the precision and stability of spectroscopic experiments.

Coherence time, as the name implies, quantifies the temporal stability of a light source's phase. More precisely, it represents the characteristic time over which the phase of the electric field remains correlated with itself. Conceptually, if one were to observe the electric field of a laser at a fixed point in space at different moments in time, the coherence time measures how long the field retains a predictable and stable relationship to its initial phase. After this interval, random phase fluctuations begin to dominate, leading to loss of coherence.

The importance of coherence time is tightly linked to laser linewidth. A longer coherence time corresponds to a narrower spectral linewidth, which is essential for resolving fine spectral features and for applications requiring high frequency stability, such as optical clocks, precision molecular spectroscopy, and quantum state manipulation.

Modern laser systems, particularly external cavity diode lasers (ECDLs), have seen remarkable improvements in coherence performance. Coherence times now routinely reach several tens to hundreds of microseconds, corresponding to coherence lengths of several kilometers. Such long coherence lengths allow lasers to serve as exceptionally stable frequency references and enable the detailed interrogation of transitions with sub-kilohertz resolution.

However, these advances also introduce new challenges in linewidth measurement. As coherence times increase, traditional linewidth measurement techniques – such as those relying on long fiber delays in self-heterodyne setups – become increasingly impractical

due to the need for extremely long delay lines, which can introduce significant optical losses and environmental noise. These challenges motivate the exploration of alternative approaches, such as short-delay self-heterodyne techniques, which this thesis aims to systematically investigate and validate.

2 Theory

To fully grasp the objective of this project, it is essential to first understand the concept of spectral line shape and linewidth – fundamental descriptors in laser physics and spectroscopy.

The spectral line shape characterizes the distribution of frequencies, or equivalently the Fourier spectrum, associated with the spectral coherence of a laser. More specifically, the line shape is typically quantified by the Power Spectral Density (PSD) of the laser's electric field or intensity.

To demonstrate how this differs from the direct Fourier transform of a signal, we modeled a 100Hz sine wave with gaussian noise, and took the both the FFT and the PSD of this signal (Fig 2.1). Here we see how powerful the PSD can be, as it describes how the power of the laser light is distributed across its frequency components, effectively illustrating both the width and structure of the spectral line [2], while the FFT spectrum is ruined by the noise.

In the most basic approximation, a laser can be thought of as a single-frequency resonator, emitting light at a discrete frequency determined by the energy difference between quantum states (Fig. 2.2). In this idealized model, the laser would produce perfectly monochromatic light with no linewidth. However, in real systems, various noise

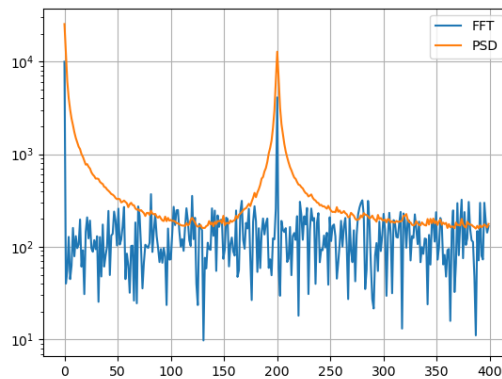


Figure 2.1: Fourier Transform and Power Spectral Density of a 100Hz Noisy Signal

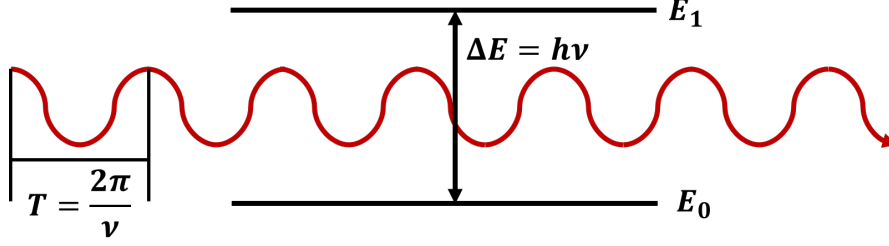


Figure 2.2: Energy Diagram of a Two Level System

sources—including thermal, mechanical, and quantum noise—broaden the spectral line, giving it a measurable width and characteristic shape. Understanding and accurately measuring this line shape is crucial for precision applications, such as frequency metrology, high-resolution spectroscopy, and quantum control experiments.

It is important to note that the application of PSD to characterize the linewidth is most commonly associated with continuous-wave (CW) lasers, as these lasers inherently exhibit long coherence times and consequently possess narrow, stable spectra.

If we assume that the laser field is dominated by a single, stable frequency then we can model the field with a single sine function:

$$E(t) = \sqrt{P_0} \sin(\omega_0 t) \quad (2.1)$$

where ω_0 is the angular frequency of the transition, and P_0 is the average intensity of the field. The frequency spectrum is the Fourier spectrum of the intensity:

$$I(\omega) = \int_{-T/2}^{T/2} |E(t)|^2 e^{i\omega t} dt = \frac{P_0}{2} \left[\delta(\omega) - \frac{\delta(\omega - \omega_0)}{2} - \frac{\delta(\omega + \omega_0)}{2} \right] \quad (2.2)$$

where T is the period we integrate over, ω is the frequency, and $\delta(\omega - \alpha)$ is Dirac delta function centered at α .

However, the direct Fourier transform provides no insight into the statistical properties or noise characteristics of the laser, which are essential for understanding real-world laser behavior. Furthermore, For optical frequencies, ω_0 typically lies in the hundreds of terahertz – far beyond the detection capabilities of conventional electronic or photonic measurement equipment.

To address the first issue, this work will present the techniques required to comprehensively characterize the random fluctuations inherent in ECDLs. It will later be demonstrated that typical linewidth of ECDLs falls within the range of approximately 1-100 kHz. To resolve the second issue, this study will also provide a detailed explanation of how the optical signal can be effectively down-converted to a radio-frequency range accessible to standard electronic measurement equipment.

2.1 Random Signal Analysis

For a perfectly monochromatic light wave, the direct Fourier transform of its electric field yields an infinitely sharp, delta-function-like spectrum. However, in practical systems, the laser frequency exhibits slight fluctuations around its nominal “center” frequency due to intrinsic noise sources and external perturbations. These frequency instabilities can be effectively modeled by introducing a time-dependent phase term into the electric field expression:

$$E(t) = \sqrt{P_0} \sin(\omega_0 * t - \phi(t)). \quad (2.3)$$

It is important to note that $\phi(t)$ originates from stochastic processes and therefore does not possess a direct analytical form. These underlying noise mechanisms limit the coherence time of the laser’s energy transition, resulting in a broadening of the spectral lineshape from an idealized infinitely sharp peak to a finite width. This spectral broadening is a direct manifestation of phase instability over time.

To accurately determine the practical laser spectrum, it is essential to introduce the concept of random signal analysis. As the name implies, random signal analysis focuses on the study of probabilistic processes and how they influence the behavior of signals over time. A key concept in this field is PSD, often referred to simply as the spectral density. The PSD is a statistical measure that describes how the power of a signal is distributed across its frequency components. Unlike the direct Fourier transform of a perfectly monochromatic signal, which yields an idealized, infinitely sharp peak, the PSD

provides a more realistic representation of the laser's total spectrum by accounting for the random fluctuations that broaden the spectral line.

The PSD, $S(f)$, discussed in this context must satisfy three fundamental conditions:

1. $S(f)$ must be a continuous function of frequency, reflecting the continuous distribution of power across the frequency domain.
2. At any specific frequency f_i , the value of $S(f)$ must be proportional to the power contribution of the original signal at that frequency.
3. The total power of the signal must be equal to the integral of the PSD over all frequencies, expressed as $P = \int_{-\infty}^{\infty} S(f) df$

In signal processing, power has a precise mathematical definition. Given a time-dependent function $x(t)$ defined over a time interval $[0, T]$, the total power P of the signal can be calculated as:

$$P = \frac{1}{T} \int_0^T |x(t)|^2 dt. \quad (2.4)$$

This expression is similar to the definition of the power of a force, but refers more generally to the power of any arbitrary time-varying signal. This definition can be easily transferred to the frequency domain by Parseval's Theorem, which states that the Fourier transform of a function must be unitary. This requires that the sum of the magnitude squared of the function in the time domain must be equal to that in the frequency domain:

$$P = \frac{1}{T} \int_0^T |x(t)|^2 dt = \int_{-\infty}^{\infty} \frac{|X(f)|^2}{T} df. \quad (2.5)$$

This definition represents the average power of the signal over the specified time period.

Using the preceding expression together with the definition of the PSD, we obtain

$$S(f) = \frac{|X(f)|^2}{T}. \quad (2.6)$$

where S_{xx} denotes the While useful, this expression provides no insight into the stochastic nature of $x(t)$. To understand why the PSD $S(f)$ is a more meaningful and practical tool

than the direct Fourier transform in this context, it is necessary to introduce a second integral, which is defined as the Fourier transform of the autocorrelation function of $x(t)$, $R_{xx}(\tau)$, [2]:

$$I = \int_{-T}^T R_{xx}(\tau) e^{-j2\pi f\tau} d\tau = \int_0^T \int_{t-\tau}^t \frac{1}{T} x(t) x^*(t-\tau) e^{-j2\pi f\tau} d\tau dt.$$

Through a change of variables $\xi = t - \tau$, this becomes:

$$\begin{aligned} I &= \int_0^T \int_0^\tau \frac{1}{T} x(t) x^*(\xi) e^{-j2\pi f(t-\xi)} d\xi dt \\ &= \frac{1}{T} \left[\int_0^T x(t) e^{-j2\pi ft} dt \right] \left[\int_0^T x^*(\xi) e^{-j2\pi f\xi} d\xi \right]. \end{aligned} \tag{2.7}$$

It's easy to see that regardless of the choice of variables, both integrals above are equal to the Fourier transform of $x(t)$. Thus, I becomes:

$$I = \frac{|X(f)|^2}{T}$$

which is the definition of the PSD. Therefore, we find that the Fourier transform of the autocorrelation is equal to the PSD.

$$S_{xx}(f) = \int_{-T}^T R_{xx}(\tau) e^{-j2\pi f\tau} d\tau. \tag{2.8}$$

This is known as Wiener-Kitchin Theorem. This theorem is highly useful in the field of signal processing, as the autocorrelation function serves as a measure of a signal's self-similarity in some time window $[0, T]$. This allows us to make quantitative statements about the stochastic processes in our signal.

2.2 Phase Noise and the Diode Lineshape

When discussing the state of a semiconductor laser, there are 3 quantities that are important to keep track of: the number of charge carriers (N), the number of photons (P), and the phase of those photons (ϕ). In fact, we actually care about the rate at which

each of these quantities change in our cavity [3]. The rate of photons in our cavity is given by

$$\dot{P} = (G - \gamma)P + R_{sp} + F_p(t) \quad (2.9)$$

where G is the net rate of stimulated emission (often just called the Gain), γ is the photon decay rate, and R_{sp} is the spontaneous emission rate. Similarly, the charge carrier rate is given by:

$$\dot{N} = I/q - \gamma_e N - GP + F_N(t) \quad (2.10)$$

where I is the current density and γ_e is the charge carrier recombination rate. Finally the rate of change of the phase is given by:

$$\dot{\phi} = -(\omega_0 - \omega_{th}) + \frac{\beta_c}{2}(G - \gamma) + F_\phi(t) \quad (2.11)$$

where ω_{th} is the threshold frequency where the cavity starts to lase, and β_c is what is called the linewidth enhancement factor. The three terms F_p , F_N , F_ϕ are what are called Langevin forces and they are stochastic terms meant to model the randomness in our cavity. F_p and F_ϕ appear due to spontaneous emission, where as F_N comes from the charge carrier recombination process.

Using small signal analysis eq 2.9-2.11 become:

$$\delta\dot{P} = -\Gamma_P\delta P + (G_N P + \frac{\delta R_{sp}}{\delta N})\delta N + F_P(t) \quad (2.12)$$

$$\delta\dot{N} = -\Gamma_N\delta N - (G + G_P P)\delta P + F_N(t) \quad (2.13)$$

$$\delta\dot{\phi} = \frac{\beta_c}{2}G_n\delta N + F_\phi(t) \quad (2.14)$$

While lasing is affected both by intensity and phase fluctuations, the lineshape is mainly shaped by the phase fluctuations. Thus, it is necessary to determine the PSD of phase $S_{\dot{\phi}}$. Using eq 2.14, we find the fourier transform of the phase rate as:

$$\delta\tilde{\phi}(\omega) = \frac{1}{i\omega}(\tilde{F}_\phi + \frac{\beta_c}{2}G_n\delta\tilde{N}). \quad (2.15)$$

This expression tells us that the linewidth manifest from two mechanisms: the first is the spontaneous emission which is represented in the Langevin force, \tilde{F}_ϕ , while second term shows the carrier population also affects the linewidth. Using eq 2.15, we can find the the PSD by:

$$S_{\dot{\phi}}(\omega) = \langle |\omega \delta \tilde{\phi}(\omega)|^2 \rangle \quad (2.16)$$

where the brackets denote the integral definition of the average of the argument. If we assume that $\delta \tilde{N}$ is dominated by the spontaneous emission term \tilde{F}_P , then an approximate solution can be obtained:

$$S_{\dot{\phi}}(\omega) \approx \frac{R_{sp}}{2P} \left(1 + \frac{\beta_c^2 \Omega_R^4}{(\Omega_R^2 - \omega^2)^2 + (2\omega\Gamma_R)^2} \right) \quad (2.17)$$

where Ω_R is the relaxation oscillation period.

As discussed in the previous section, if we want to know what the natural lineshape of a laser is, we must find the PSD of the electric field. Using Equation 2.8 we find:

$$S_E(\omega) = \int_{-\infty}^{\infty} \langle E^*(t + \tau) E(t) \rangle e^{i\omega\tau} d\tau. \quad (2.18)$$

For the purpose of our derivation, we assumed that power fluctuations are small enough to not effect the field, in which case, the field is given by:

$$E(t) = P^{1/2} e^{-i(\omega_0 t + \phi + \delta\phi)} \quad (2.19)$$

where $\delta\phi$ is a small change in the phase and ω_0 is the center frequency of the emitted light. Thus plugging in eq 2.10 into 2.9, we find:

$$S_E(\omega) = \int_{-\infty}^{\infty} \langle e^{i\Delta_\tau\phi} \rangle e^{-i(\omega - \omega_0)\tau} d\tau \quad (2.20)$$

where

$$\Delta_\tau\phi = \delta\phi(t + \tau) - \delta\phi(t). \quad (2.21)$$

The expectation value of $e^{i\Delta\phi}$ can be determined by assuming the probability density

function is a gaussian. In which case we can use the identity that the Fourier transform of a gaussian is another gaussian in the new variable [4]:

$$\langle e^{i\Delta_\tau\phi} \rangle = e^{-\frac{1}{2}\langle(\Delta_\tau\phi)^2\rangle} \quad (2.22)$$

It is beneficial to look at the Fourier transform of Eq 2.12:

$$\Delta_\tau\phi = \frac{1}{2\pi} \int_{-\infty}^{\infty} \delta\phi(\omega)(e^{i\omega(t+\tau)} - e^{i\omega t})d\omega \quad (2.23)$$

and because the cross correlation between different frequencies is zero we find:

$$\langle(\Delta_\tau\phi)^2\rangle = \frac{1}{\pi} \int_{-\infty}^{\infty} \langle|\Delta_\tau\phi(\omega)|^2\rangle(1 - \cos(\omega\tau))d\omega. \quad (2.24)$$

Using eq 2.16, the expression above becomes

$$\langle(\Delta_\tau\phi)^2\rangle = \frac{1}{\pi} \int_{-\infty}^{\infty} S_{\dot{\phi}}(\omega) \frac{(1 - \cos(\omega\tau))}{\omega^2} d\omega. \quad (2.25)$$

. Plugging in eq 2.17 would still result in an unwieldy expression, but if we assume the relaxation oscillations are much faster than the center frequency, then we can assume $S_{\dot{\phi}}(\omega)$ is constant. In which case, we find:

$$\langle(\Delta_\tau\phi)^2\rangle = \tau S_{\dot{\phi}}(0) \quad (2.26)$$

Taking this result we find that 2.20 becomes:

$$S_E(\omega) = P \int_{-\infty}^{\infty} e^{i(\omega_0 - S_{\dot{\phi}}(0)/2)\tau} e^{-i\omega\tau} \quad (2.27)$$

This expression is the Fourier transform of a Lorentzian centered at ω_0 with a linewidth of $S_{\dot{\phi}}(0)$. In terms of linewidth in Hz, we find:

$$\Delta f = \frac{R_{sp}}{4\pi P}(1 + \beta_c^2). \quad (2.28)$$

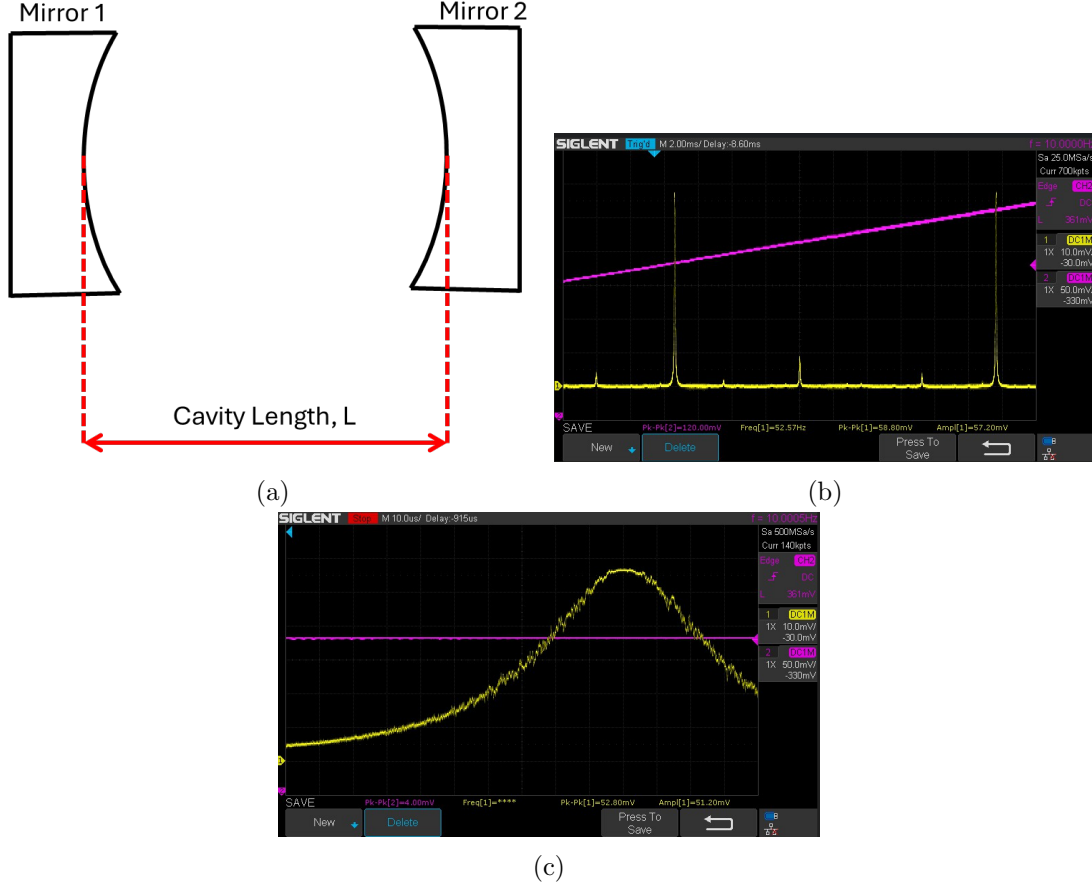


Figure 2.3: (a) Fabry Perot Cavity, (b) Cavity Transmission, (c) Zoom in of a Transmission Peak

The value $\frac{R_{sp}}{4\pi P}$ is referred to as the Schawlow-Townes limit for a diode laser. This is a historically important value as the Schawlow and Townes were the first to derive the linewidth of CW lasers, particularly ammonia masers, and this is the result one would find through their methods [5]. Here we find that the linewidth is further narrowed by a factor of $1 + \beta_c^2$ which is where β_c gets its name.

2.3 Beat note Generation and Linewidth Extraction

The expression for the linewidth found in the previous section is very useful in outlining the fundamental limit of semiconductor laser coherence. As useful as it is, the fundamental linewidth of a laser is very hard to measure directly, as ω_0 is often far outside the range of any electrical measuring device.

There are many ways of determining the linewidth of optical light. The most direct

way is to use a diffraction grating and measuring the linewidth directly from the interference intensity pattern, but the spectral resolution here is very limited. A better way is to use what is called a Scanning Fabry-Perot (FP) interferometer (Fig 2.3a). This is a resonant cavity made of two parallel, highly reflective, concave mirrors. Light at resonance exhibits a large peak in the transmission signal, and as the cavity length is changed or "scanned" the transmission signal quickly dies off. The problem with this kind of measurement is that the spectral resolution is highly dependent on the Free Spectral Range (FSR) and the Finesse of the cavity [6]

$$FWHM = \frac{\nu_{fsr}}{F} \quad (2.29)$$

FSR is the frequency spacing between resonant modes in the cavity,

$$\nu_{fsr} = c/(2L) \quad (2.30)$$

where c is the speed of light and L is the cavity length. The FSR is visualized in Fig 2.3b as the two large transmission peaks. Meanwhile, finesse tells one how defined a spectral feature can be (Fig 2.3c) and is determined by the cavity reflectivity, r :

$$F = \frac{\pi\sqrt{r}}{1-r}. \quad (2.31)$$

From this, one can see that the spectral resolution is highly dependent on the choice of mirrors. For instance, a 5cm cavity with two mirrors of .99 reflectivity has a spectral resolution of 10MHz. While good for some applications, modern CW diode lasers can easily get linewidths in the kHz range.

In this section, we will discuss a robust approach to measuring linewidths for a large range of values, including values well below any reasonable FP measurement. While the two previous techniques are based on creating a spatial interference pattern, the main technique that we will discuss is based on beat-note generation, which is a temporal interference pattern.

The techniques of interest here are homodyning and heterodyning. Both methods involve combining two signals at a photodetector and measuring the time-dependent, phase-induced interference. With a homodyne measurement, the two signals are of the same frequency, while the heterodyne technique uses two signals near the same frequency but with one signal being slightly higher than the other (Fig 2.4).

When beating signals of equal frequencies, the resulting beat signal has the same frequency but the amplitude changes as a function of the relative phase. This is what one would expect for low frequency homodyning, but due to the high frequencies of optical light the actual measured signal is a DC signal with the phase resulting in slight fluctuations on the DC level.

With the heterodyne technique, signal is a mix of the two signals but due to the main THz frequency, the signal is dominated by the frequency difference Δf . This results in almost a pure sinusoidal signal with frequency Δf where the relative phase modulates the amplitude of the signal.

The purpose of these techniques is to downconvert the noise spectrum of the laser into a measurable range, with the homodyne method converting it to the near DC range, and the heterodyne technique converting the signal to the tens of MHz range. While both techniques seem comparable, heterodyning is usually the more preferable technique. This is because most detectors have a much higher noise floor near DC, a phenomena called flicker noise or $1/f$ noise. This high noise floor means that the signal-to-noise ratio of a homodyne measurement is much worse than that of a typical heterodyne measurement [7].

Up until now, the spectrum discussed does not resemble the simple Lorentzian profile as one would expect. In general, beat-note techniques do not return the exact laser spectrum. They can produce direct spectra in the case where the delay time is very long, but the connection between the spectra above and the laser linewidth is obscure up to this point.

Deriving any power spectral density starts with the equation of field at the detection point. As seen in fig 2.4b, the field is going to be the sum of two sinusoidal fields with

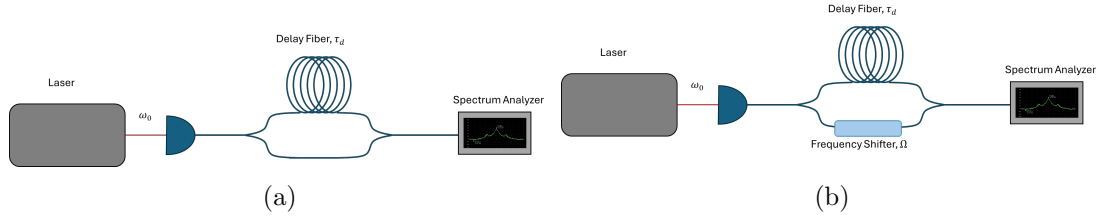


Figure 2.4: (a) Self Homodyne Technique, (b) Self Heterodyne Technique

frequencies f_0 and $f_0 + \Delta f$, where f_0 is the center frequency of the laser. Due to splitting the field down two arms, in general there will be a phase caused by the time delay, τ_d , of the two fields, thus the total field at the detector is:

$$E(t) = \sqrt{P_0} \cos(\omega_0 t + \phi(t)) + \sqrt{P_0} \cos((\omega_0 + \Omega)(t - \tau_d) + \phi(t - \tau_d)) \quad (2.32)$$

where P_0 is the total power at the detector, and ω_0 and Ω are 2π times f_0 and Δf respectively.

The photodetector does not measure fields but instead produces a voltage proportional to the intensity of the field, thus the intensity derived from the equation above is:

$$\begin{aligned} I(t) &= |E(t)|^2 \\ &= P_0 [\cos^2(\omega_0 t + \phi(t)) + \cos^2((\omega_0 + \Omega)(t - \tau_d) + \phi(t - \tau_d)) \\ &\quad + 2\cos(\omega_0 t + \phi(t))\cos((\omega_0 + \Omega)(t - \tau_d) + \phi(t - \tau_d))]. \end{aligned}$$

Using the well known product of cosines identity, $I(t)$ becomes:

$$\begin{aligned} I(t) &= P_0 [\cos^2(\omega_0 t + \phi(t)) + \cos^2((\omega_0 + \Omega)(t - \tau_d) + \phi(t - \tau_d)) \\ &\quad + \cos(2\omega_0 t - \Omega t - (\omega_0 + \Omega)\tau_d + \phi(t) + \phi(t - \tau_d)) \\ &\quad + \cos(-\Omega t + (\omega_0 + \Omega)\tau_d + \phi(t) - \phi(t - \tau_d))]. \end{aligned}$$

Since ω_0 is such high frequency, any component with a $\omega_0 t$ term will only contribute as

their time averages. Thus, the first two terms will average to 1/2 while the third term averages to 0. Therefore, the measured intensity at the detector is:

$$I_d(t) = P_0(1 + \cos(-\Omega t + (\omega_0 + \Omega)\tau_d + \phi(t) - \phi(t - \tau_d))).$$

The expression above is important because it solves the two main flaws Eq. 2 had:

1. this expression preserves the phase noise information in the form of $\phi(t)$ and $\phi(t - \tau_d)$
2. the Ωt dependence means the noise spectrum has been shifted away from the THz range down to a set frequency difference which can easily be made to be in the bandwidth of our detector.

With the photodetector intensity, we can find the auto-correlation function [8]:

$$R_{xx}(\tau) = \frac{1}{2}P_0^2 \cos(\Omega\tau) \langle \cos(\Delta\phi(\tau, 0) - \Delta\phi(\tau - \tau_d, \tau_d)) \rangle$$

with the bracket denoting the expectation value, and where $\Delta\phi(t_1, t_2)$ is the phase difference between t_1 and t_2 , $\phi(t + t_1) - \phi(t + t_2)$.

Recalling from eq 2.22, if the phase noise is assumed to have a gaussian probability, then $\langle \cos(\Delta\phi) \rangle = e^{-\langle \Delta\phi^2 \rangle / 2}$. If we also assume that the phase noise PSD (eq 2.26) then we find:

$$R_{xx}(\tau) = \frac{P_0^2}{2} e^{-|\tau_d|/\tau_c} \cos(\Omega\tau) e^{-\frac{1}{\tau_c}(\tau - |\tau_d|)} \quad (2.33)$$

Here we see that if the coherence time is much shorter than the delay time, then the auto correlation function resembles the Fourier transform of a Lorentzian (eq 2.27). Here is precisely why it is often chosen to use very long delay fiber to do linewidth extraction. The resulting PSD should result in a Lorentzian that is straight forward to fit.

This thesis, on the other hand, is interested in the advantages of using much shorter delay times than the coherence length of a laser to extract the PSD. Doing the Fourier

transform of eq 2.33 results in:

$$S(\omega) = \frac{1}{2} \frac{P_0^2 \tau_c}{1 + (\omega \pm \Omega) \tau_c^2} \left\{ 1 - e^{-|\tau_d|/\tau_c} \left[\cos(\omega \pm \Omega) |\tau_d| + \frac{\sin(\omega \pm \Omega) |\tau_d|}{(\omega \pm \Omega) \tau_c} \right] \right\} + \frac{1}{2} P_0^2 \pi e^{-|\tau_d|/\tau_c} \delta(\omega \pm \Omega). \quad (2.34)$$

Again, we see that if coherence time is small then we get an approximate Lorentzian. But when coherence time and delay times are comparable, we get this oscillatory "coherence side lobes."

A more commonly used expressions in this field is given in terms of frequency below [9]:

$$S(f) = S_1 * S_2 + S_3 \quad (2.35)$$

$$S_1(f) = \frac{P_0^2}{4\pi} \frac{\Delta f}{\Delta f^2 + (f - f_1)} \quad (2.36)$$

$$S_2(f) = 1 - e^{-2\pi\tau_d\Delta f} \left[\cos(2\pi\tau_d(f - f_1)) + \Delta f \frac{\sin(2\pi\tau_d(f - f_1))}{f - f_1} \right] \quad (2.37)$$

$$S_3(f) = \frac{\pi P_0^2}{2} e^{-2\pi\tau_d\Delta f} \delta(f - f_1) \quad (2.38)$$

This expression directly gives us the linewidth Δf . Notice that $S(f)$ includes a delta function S_3 . This delta function can make precise fitting tricky. This feature is also highly susceptible to electronic noise, making it a fit to eq 2.38 even more difficult. In section 4.2 we will propose a modification to S_3 that makes fitting easier.

3 Experiments

The purpose of this thesis is to demonstrate the effectiveness of introducing a temporal delay using an optical fiber whose length is well within the laser's coherence time. In contrast to the conventional approach, which utilizes long optical fibers to induce phase delays exceeding the coherence time, this method enables a more compact design.

The main advantage of sub-coherent self-heterodyne detection is that it reduces fiber-induced $1/f$ noise. Fiber induced noise is a phenomena where temperature and vibration induced fluctuations in the fiber length or index of refraction induce a phase in the light traveling through the fiber. This noise is separate from the inherent noise of the laser, and increases with delay fiber length [10]. The inclusion of this noise broadens the apparent laser spectrum, and often requires a fitting to Voigt when fibers longer than the the coherence length of the laser is used.

3.1 Self-Heterodyne Design

Based on the discussion of the PSD in section 2.3, there are two key components necessary for generating the heterodyne spectrum. The first component involves creating a phase delay, using a long optical fiber. The other necessary component requires generating a frequency difference of the beating signals to eliminate the DC noise. To accomplish this frequency difference in the optical range, an acousto-optic modulator, or AOM is used.

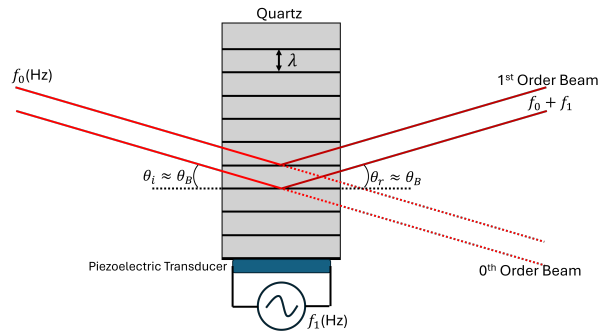


Figure 3.1: AOM Diagram

An AOM is a device composed of a transparent medium, typically quartz, and a piezoelectric transducer, PZT, as shown in figure 3.1. The PZT is a ceramic component that expands and contracts in response to an applied voltage. Applying an AC signal to the PZT while it is in contact with the quartz creates sound waves in the material. These waves affect the density and thus create areas of high and low index of refraction. This modulated index of refraction makes the AOM act as a transmission grating, deflecting the beam as shown in fig 3.1. Because this diffraction is induced by a moving wave, the diffracted wave is Doppler shifted by the wave frequency:

$$f = f_0 + mf_1 \quad (3.1)$$

where m is the diffraction order. Including the AOM means we can beat the laser with itself, which inherently means the noise spectrum down both arms are identical. If the AOM was not included, then one would need a laser with smaller noise spectrum, detuned slightly from f_0 , in order to only measure the noise spectrum of the studied laser.

As shown in figure 3.2, the light is split down two arms using a polarizing beam splitter, PBS. This, in combination with a half-waveplate, HWP, allows us to control the ratio of light down each arm. This is because the PBS splits light based on whether it is parallel or perpendicularly polarized, and the HWP rotates the polarization. After the PBS, some of the light is sent through the delay fiber and some is sent through the AOM. The delay fiber was chosen to be a single mode telecom fiber, as long fibers in this regime are typically cheap. This also means we expected losses in the delay fiber due to coupling inefficiencies. The light sent through the AOM is deflected slightly but still has some chance of interacting with the photodetector, so an iris ensures the best isolation between the 0th and 1st order. After the delay fiber, a second HWP is used to match the polarization of the two arms for optimal interference. Because the light has to be recombined without influence from the polarization of either beam, a non-polarizing beam splitter, NP-BS, was used. Finally, the signal from the photodetector is sent to a TinySA Ultra spectrum analyzer which outputs the PSD. The AOM used was an IntraAction Corp AOM with a 40MHz center frequency, driven by a Minicircuit ZHL

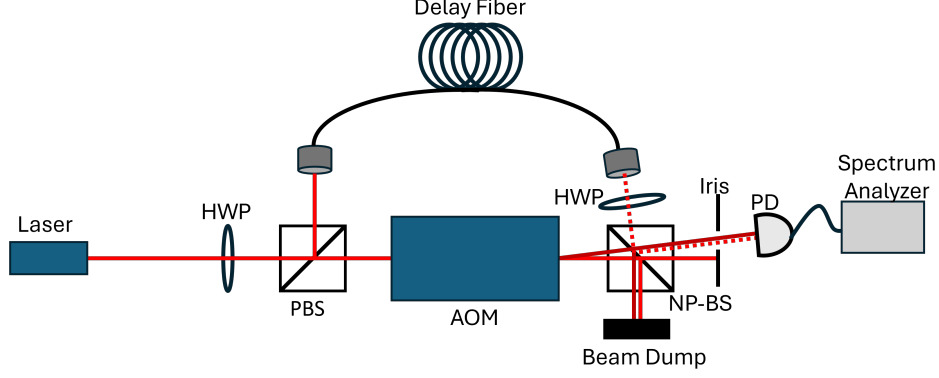


Figure 3.2: Experimental Setup of Self heterodyne Experiment

1-2W+ RF amplifier.

The expression found in the previous section gives some insights into how long of a fiber should be chosen for a given measurement. Using Eq 2.35, it can be seen that different linewidths can influence the the contrast between adjacent extrema, as seen in Fig 3.3. Here we see the plot of $S_1 \times S_2$ for two different linewidths using the same delay time.

This plot shows that linewidth serves mainly to decrease the size of the of the coherent sidelobes. The improved contrast between x and y implies that a better measurement could be extracted for the 10 kHz linewidth using a subcoherent approach than could be done for the 100 kHz linewidth. This runs counter to the incoherent approach, where smaller linewidths imply worse relative resolution, and thus more uncertainty [11].

To further show how, using Eq 2.35, we made a plot of the contrast between the first minima and maxima after the main lobe. This comparison was made for multiple delay fiber lengths as shown in fig 3.4. Here we see that contrast is generally higher for shorter fibers. The intersection with the line at 0dBm represents where $\tau_d < \tau_c$. This is roughly where the Lorentzian term starts to dominate in our expression, Eq 2.35.

3.2 ECDL Design

As a way of verifying the results of our instantaneous linewidth extraction, we chose to compare the linewidth of a laser to a well known and easily resolvable transition. For this

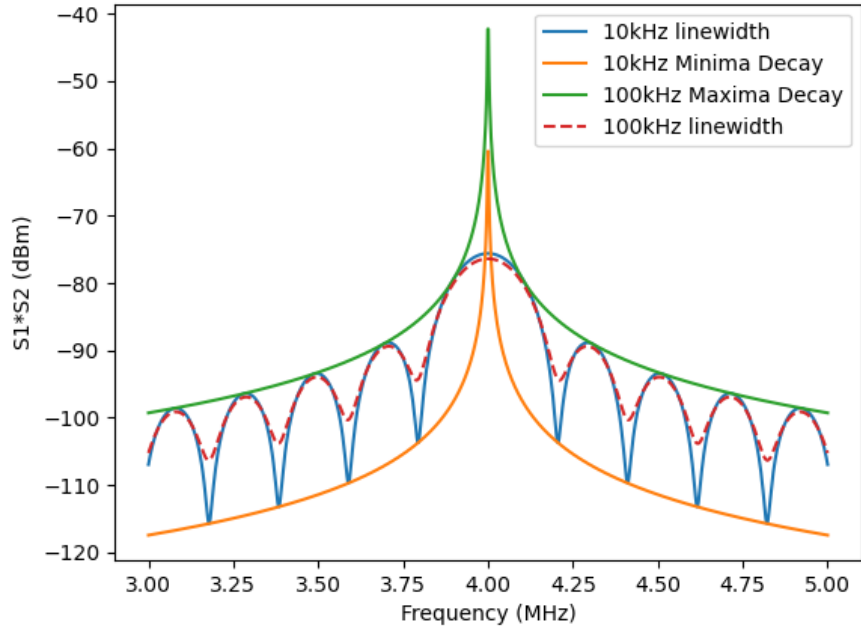


Figure 3.3: Comparison of PSD Size for Different Linewidths

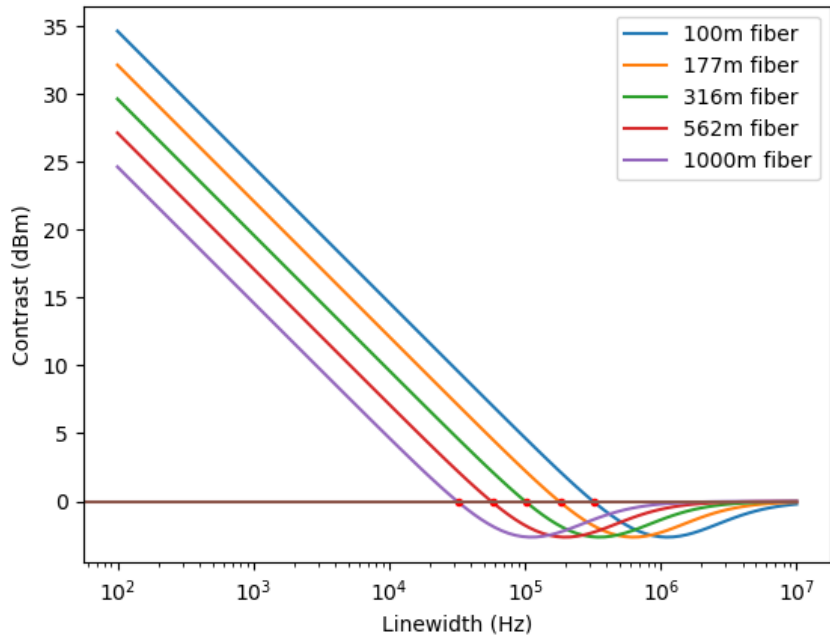


Figure 3.4: Plot of Extrema Difference as a Function of Linewidth

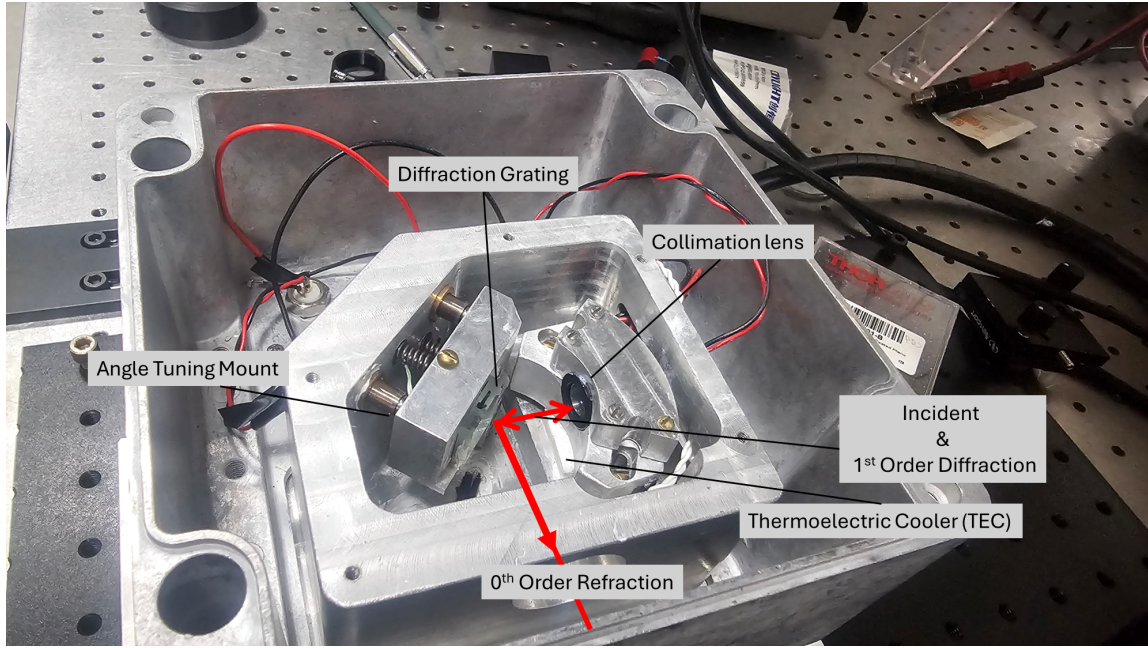


Figure 3.5: 780 nm ECDL

reason we chose the D-line transitions of ^{87}Rb . The precise transitions and the reason for choosing these will be explained in section 3.4.

In order to interrogate the specific transitions we are looking at, we required a laser centered around 780 nm. This laser also had to be capable of producing linewidths narrower than the transition lifetime. For this reason we chose to build an External Cavity Diode Laser (ECDL) with a 780 nm laser diode as the gain medium.

The ECDL is a common diode laser design that is meant to improve the stability of a bare laser diode. A bare laser diode works in a way similar to a Fabry Perot Cavity (2.2a), where the reflective facets of the laser serve select and narrow a specific frequency.

The Fabry Perot laser is flawed in two main ways:

1. The cavity size L is on the order of a diode chip (5 mm), which makes mode spacing relatively large according to 2.10, but FWHM increasing in proportion.
2. The small size makes it hard to servo L , meaning frequency selectivity is almost entirely dependent on the diode current.

The ECDL is designed to correct these flaws. As seen in Fig 3.5, the ECDL is composed

of a laser diode, a collimation lens, and a diffraction grating. Unlike the FP Laser, where both the front and back facets of the chip were high reflection (HR) coated, here the front facet is anti-reflection (AR) coated. This means very little of the amplification comes from the internal diode cavity. Instead, a diffraction grating redirects the light out of the diode, according to the grating equation:

$$a(\sin(\theta_m) + \sin(\theta_i)) = m\lambda \quad (3.2)$$

The precise design we used is called the Littrow Configuration. This is where the grating angle is set so that the first order, $m = 1$, beam is reflected back into the diode, $\theta_i = \theta_1$, which simplifies the grating equation significantly [12]:

$$\lambda = 2a\sin(\theta_i). \quad (3.3)$$

This makes a resonant cavity with the HR back facet of the diode and the Partially Reflective (PR) face of the grating. From equation 3.3, we can see that we no longer need current or cavity length control for frequency selectivity. Instead, we can rotate the grating to choose the lasing frequency of the cavity. The increased cavity size (5cm) also serves to reduce the linewidth by at least two orders of magnitude.

While the ECDL can reduce the phase noise in the laser, extending the cavity size makes the cavity much more susceptible to temperature induced noise. To reduce temperature effects, our cavity design has two thermoelectric coolers (TECs), which can be seen in under the lens mount in Fig 3.5. Our ECDL is made of two independent, aluminum housings; the internal housing is the cavity itself with the grating and diode housed inside, while the outer housing is meant to isolate the cavity from the lab environment.

The first TEC is placed under the cavity housing and is meant to temperature stabilize the cavity as a whole. As the temperature rises, the cool side of the TEC cools the cavity and uses the large thermal mass of the outer shell as a heat sink. This, in theory, should eliminate the temperature induced cavity length drift.

The second TEC, on the other hand, is meant to eliminate phase noise from the diode

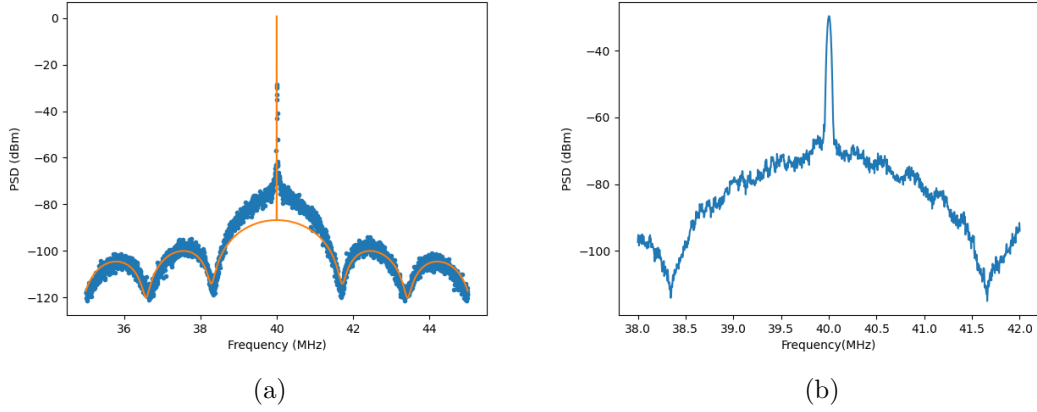


Figure 3.6: (a) Example of PSD using 120 m Delay Length, (b) Zoom in of Delta Feature

that is caused by the temperature dependent index of refraction of the diode. This TEC is placed right below the diode mount and works much in the same way as TEC 1.

TEC 1 and 2 are independently monitored by dedicated thermistors mounted near the desired servo-ed mass. Each TEC-thermistor pair forms a thermal loop, which provides an output and input to a Proportional-Integral-Gain (PID) controller respectively. The PID monitors the temperature error ΔT , given by $T_{set} - T_{thermistor}$, and drives the TEC to reduce ΔT to 0. The PID is tuned using a Zigler-Nichols approach to quickly drive the temperature to T_{set} .

3.3 Fitting Procedure

All free running linewidths presented in this paper were extracted by doing a global fitting using a nonlinear least square fit to the PSD equation, although the final equation used was not the exact PSD derived in 2.3.

There are two main issues with using the exact expression for the self heterodyne PSD. The first issue is demonstrated in fig 3.6a. Here we see a fit to the data that reliably reproduces the sidelobes, but does not fit the center delta feature. For multiple reasons, the delta feature never matches theoretical predictions [9], [13]. The second issue is revealed by doing a short range scan of the PSD (Fig 3.6b). This scan was done with a resolution bandwidth of 30 kHz, and at this resolution we see that the delta feature is

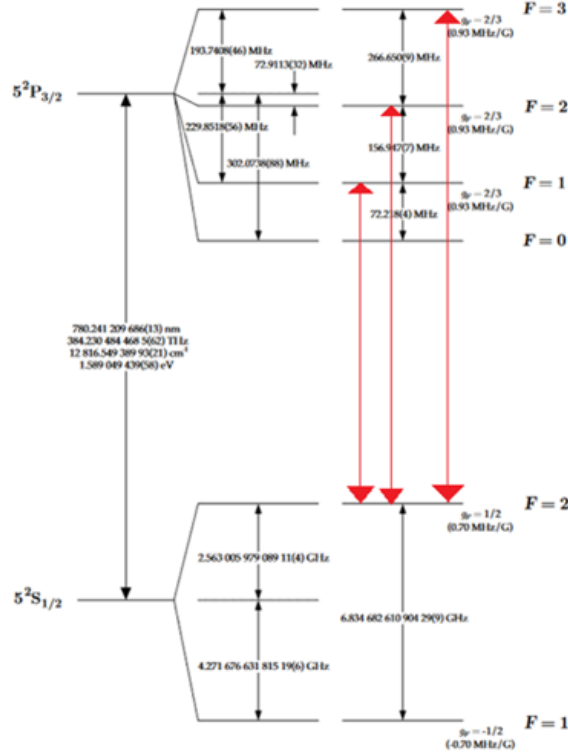


Figure 3.7: Diagram of ^{87}Rb D-line Transitions

significantly broadened. We will see later that this broadening becomes more severe as resolution bandwidth increases.

For these reasons we replaced the S3 therm is the PSD with an arbitrary function that is derived in section 4.2.

3.4 Rb Spectroscopy

As a benchmark test for our linewidth estimation, we decided to compare the free-running linewidth of our 780 nm ECDL to hyperfine transitions of ^{87}Rb . ^{87}Rb was the first molecule used to create a Bose-Einstein Condensate (BEC). This fact has made it the source of multiple studies, and as such made the optical spectrum of ^{87}Rb very well known. This, combined with the relatively large absorption coefficients and moderate lifetimes of transitions near 780 nm, makes ^{87}Rb a good candidate for a reliable optical, absolute reference.

The specific transitions are the D-line transitions of ^{87}Rb shown in red in Fig 3.7 [14].

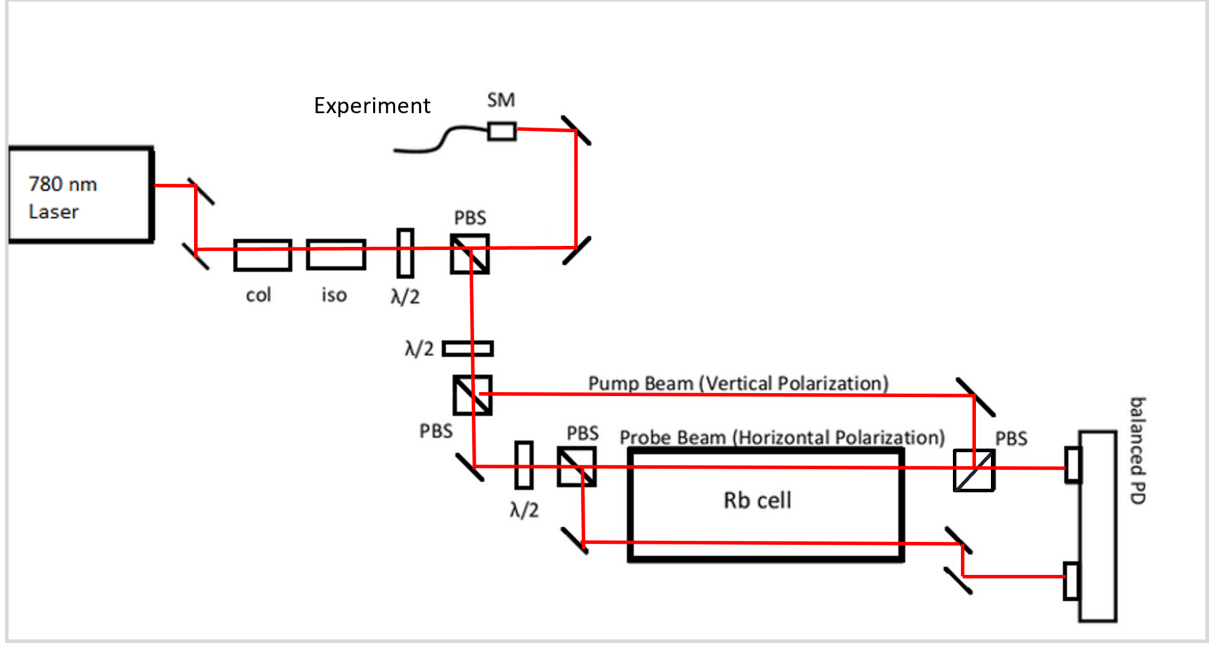


Figure 3.8: Saturated Absorption Scheme Used for Measuring ^{87}Rb Transitions

These transitions have a linewidth of 6MHz, but center of the transition can be measured to much higher resolution through Frequency Modulate (FM) Spectroscopy.

The way we measured these narrow transitions was through saturation absorption spectroscopy as shown in Fig 3.8. This approach allows us to measure the Doppler free spectrum of ^{87}Rb , but also produces crossover transitions caused by overlap of different Doppler shifted transition. This means our spectrum has 3 extra peaks at the average frequency of two real transitions [15].

By modulating the current to the diode, we were able to modulate the laser frequency as the expression shown below:

$$E(t) = E_0 e^{i\omega_0 t + i\beta \sin(\omega_m t)} \quad (3.4)$$

where β is the modulation amplitude and ω_m is the modulation frequency.

This equation can be expressed as an expansion of Bessel functions [1]:

$$E(t) = E_0 \sum_{n=-\infty}^{+\infty} J_n(\beta) e^{i(\omega_0 + n\omega_m)t} \quad (3.5)$$

where J_n is the nth order Bessel function. The end result of this type of scheme is that

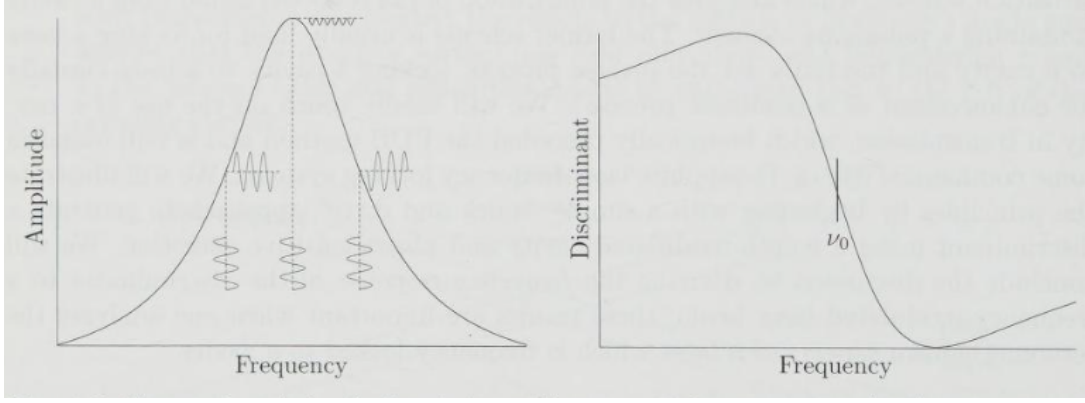


Figure 3.9: Graphic of Derivative of Transition Discriminant Generation [1]

an anti symmetric lock point is generated by frequency modulation.

When the laser scans over the resonance of the transition, the modulation has very little effect on the transmission through the cell, due to the symmetry and small curvature at the peak. Meanwhile, at the inflection points of the transition, the curvature is large so the transmission experiences the largest effect near these points. The slope on either side of the transmission has opposite signs, so the transmission will have opposite signs which results in a the antisymmetric signal shown in figure 3.8. Functionally, the reaction of the transition to a modulating signal converts the frequency modulation into amplitude modulation.

This can be used to reliably measure the linewidth of a transition, but it typically requires small values of β . This is because when β is small, and thus the size of the modulation away from resonance is small compared to the FWHM, then the intensity measured by the photodetector will have the form:

$$I_d(\omega) = I_d(\omega_0) + \left. \frac{dI_0}{d\omega} \right| (\beta \sin(\omega_m t)) \quad (3.6)$$

Therefore, in the limit that β is smaller than the FWHM, we can assume the transmission signal is proportional to the derivative of the natural shape of the transition. The antisymmetric shape of the derivative provides a more precise estimate of the transition crossing, and also opens up the possibility of servo-ing the laser current to center of the transition.

4 Results

4.1 Rb Locking and the ECDL Upper Bound

The purpose of conducting frequency modulated spectroscopy of ^{87}Rb was to set an upper limit on the free-running linewidth of the 780 nm ECDL. This would serve as a measure of the reliability of our self heterodyne measurements.

Above is an image of the hyperfine spectrum discussed in section 3.4 as observed on a oscilloscope, along with the derivative signal generated by frequency modulating our laser. The orange trace was generated by applying a ramp to the current, which allowed us to sweep the center frequency of the laser. To get the best possible lock, the ramp had to be small enough to contain only one spectroscopic feature, as shown in fig 4.1b. The ramp rate at this instance was measured to be 863 mV/ms.

Assuming that each spectroscopic feature is a Lorentzian, as one would assume for the natural lineshape of an atomic transition, then the distance between the maximum and minimum of the derivative is related to the natural linewidth by:

$$\Delta f' = \frac{\sqrt{3}}{3} \Delta f \quad (4.1)$$

where Δf is the the linewidth of the Lorentzian. Assuming the linewidth is 6MHz, then

$$\Delta f' \approx 3.5 \text{ MHz}$$

Dividing the $\Delta f'$ by the measured time between minimum and maximum, we got frequency rate of 14 MHz/ms. Dividing our ramp rate by this frequency rate gave us a conversion factor of 16 kHz/mV. This conversion factor is important because it allows to convert the electrical signals measured by our photodetector into the frequency of our laser.

Once the laser was locked, we measured and error signal of 1.5mV RMS. This trans-

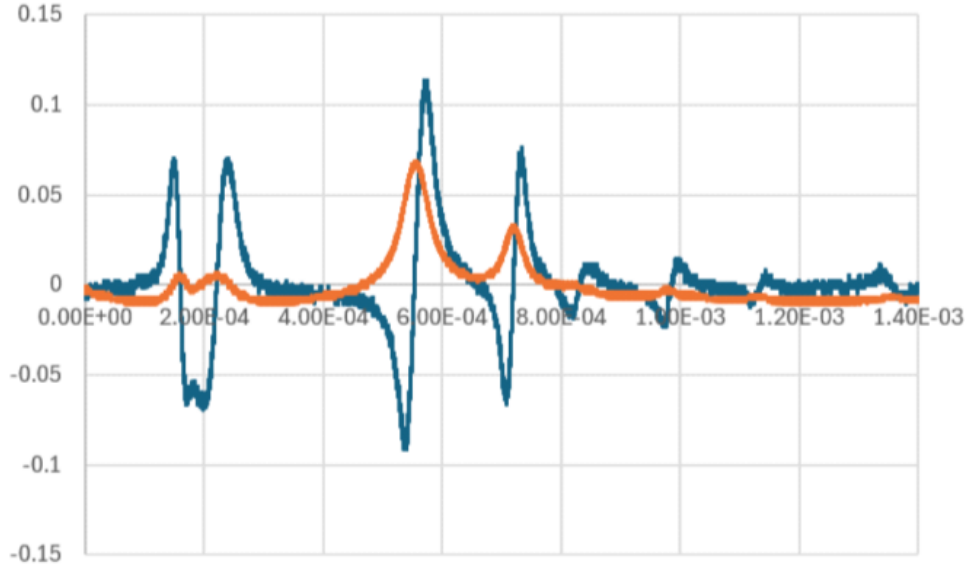


Figure 4.1: Experimentally Observed ^{87}Rb Transitions (Orange) and the FM Generated Derivative (Blue)

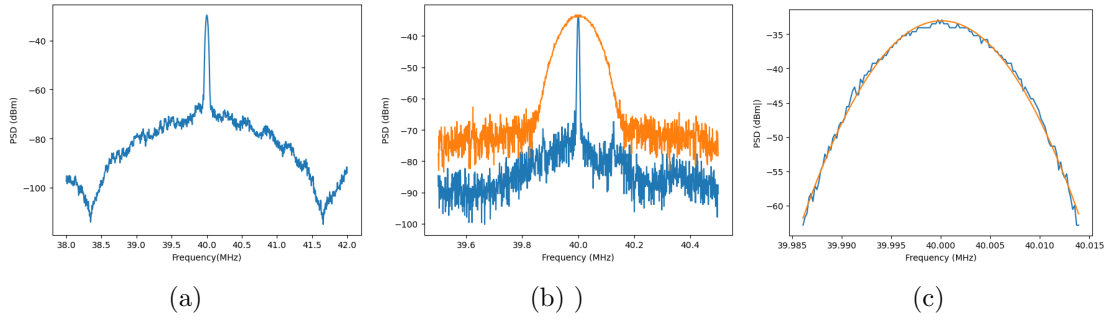


Figure 4.2: (a) Zoom-in of Delta Feature, (b) Comparison of Delta Feature Response to Different Resolution Bandwidths (30 kHz in orange, 3 kHz in blue, (c) Fitting of the Delta Feature to a Gaussian of Width Equal to RBW

lates to a locked linewidth of 24 kHz. This result is the upper limit of our possible measured linewidth by the self heterodyne measurement. This is the upper bound because a low signal to noise ratio could make the locking linewidth larger than the natural linewidth, or residual amplitude modulation (RAM) could broaden the derivative signal [16]. The latter is very likely because the modulation depth in our case was relatively large.

4.2 Noise Floor and Window Function Modeling

An important step in the process of linewidth extraction was establishing the limitations of our spectral analyzer. As mentioned before, we used a TinySA Ultra.

Spectrum analyzers are devices meant to measure an approximate spectrum known as a periodogram [17]. This works by sectioning off the spectrum into multiple frequency bins and then sweeping a filter over each bin. By doing this it calculates the truncated PSD of each bin and then stitches the signal back together at the end.

An important feature in this kind of PSD is the shape of filter used to window the spectrum. Fig 4.2a shows a close up measurement of the subcoherent PSD centered at the AOM frequency of 40 MHz. The subcoherent PSD equation states that at 40 MHz we expect to see a sharp delta feature, but as seen in Fig 4.2a there is a broadening of that feature. That broadening is caused by the finite size of the window. This is called the Resolution Bandwidth (RBW). Thus, for modeling, it is more effective to replace the delta feature with the window function.

Fig 4.2b shows the 'delta' feature with a 100kHz and 10kHz RBW, for the same signal. It is important to note that the feature narrows as the RBW decreases. It should also be noted that the choice of window affects the offset of the signal.

We assumed that the window function chosen by the manufacturers of the TinySA was a gaussian:

$$f(x) = ae^{-\frac{4\ln(2)(x-x_1)^2}{FWHM^2}}$$

where FWHM is the full-width half max of the gaussian and x_1 is the center position. Since the spectrum analyzer displays results in dBm, we used the following quadratic expression for ease in fitting:

$$Window(f) = a + \frac{10}{\log 10} \frac{4\ln 2}{FWHM^2} (f - f_1)^2. \quad (4.2)$$

Figure 4.2c shows this fitting function over just the truncated PSD that contains the broadened delta.

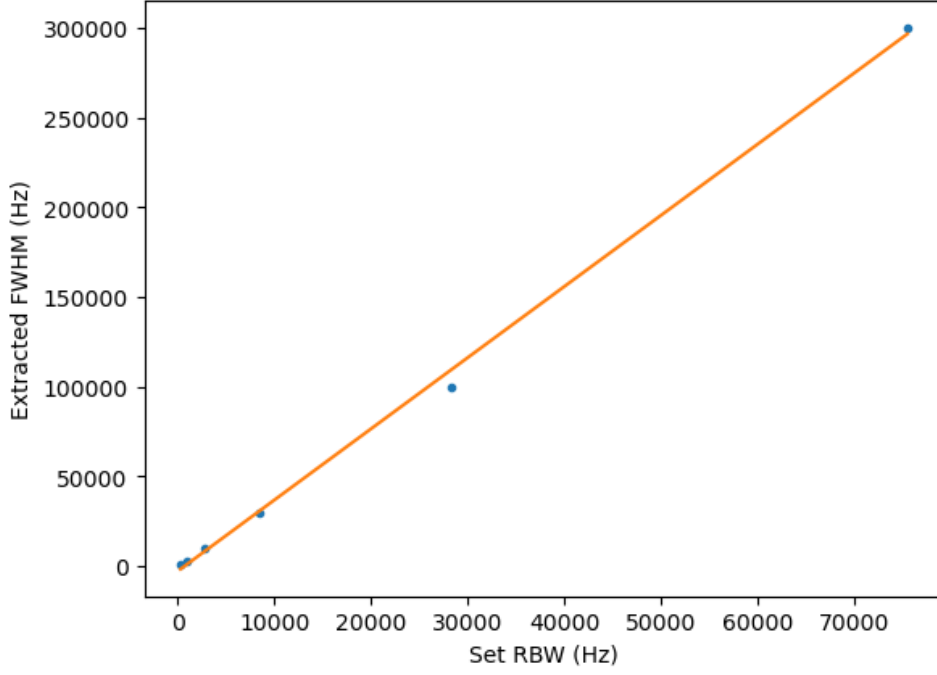


Figure 4.3: Comparison of Extracted Delta Feature Width and Set RBW

From our fit equation, we extracted the FWHM for multiple RBWs and plotted them against each other as shown in fig 4.3. Doing a linear fit to this data, we extracted a slope of 1.2. The factor of $4\ln 2$ is particular to the width of a gaussian, so the fact that we got 1.2 as our slope indicates that our assumption to model the window as a gaussian was accurate.

As mentioned before, the choice RBW affects the noise level, as seen in Fig 4.2a. This is due to the noise floor of the detector changing with RBW. The noise floor is the smallest possible signal that can be measured. If we were to try to measure the PSD past the noise floor we would see a truncation of our signal, which would affect our final linewidth estimate [7].

The noise floor was measured by terminating the spectrum analyzer with a $50\ \Omega$ terminator, to measure just the noise of the detector itself. The smallest noise floor was measured to be 110 dBm, so any measurement that was near that floor had to be amplified with a low noise amplifier.

We also notice that while RBW affects the noise level, it does not change the size of the actual noise. Determining the noise envelope was necessary as certain features of the

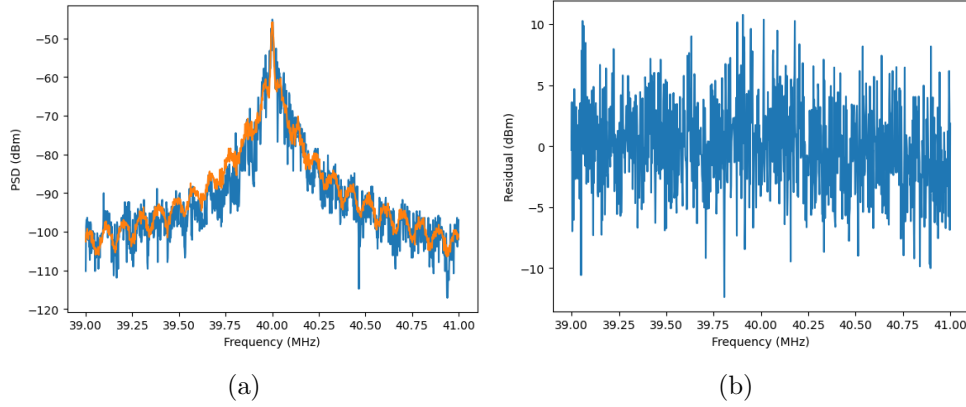


Figure 4.4: (a) Comparison of Noise Level for a Single Scan at 10 kHz RBW (Blue), and Average of 16 Measurements (Orange), (b) Residual of Average and Single Scan

PSD could be obscured by the noise.

In order to determine the noise power in our system we measured the PSD of the 780 nm laser through a 2 km fiber with a 10 kHz RBW. This measurement was done 16 times back to back as shown in figure 4.4a.

We assumed the average represented the real noise free PSD and took the residual between the average and a single scan, as seen in Fig 4.4b. Taking the standard deviation of the residual, we found the noise power of single measurement to be 3dBm. This means that resolving any feature in our PSD requires either more than 3dBm contrast or averaging of multiple measurements.

4.3 Linewidth and Delay Time

As mentioned before, this paper accesses the effectiveness of our fitting procedure by using three different lasers: a 950 nm DFB laser, a home built 780 nm ECDL, and a turn-key 720 nm DL Pro Laser from Toptica. These three lasers were measured with both a 120 m and 2 km delay fiber.

Since the best way to establish the precision of a laser is through comparison to a fixed, high precision, atomic source, the most important laser to quantify was the 780 nm ECDL. This is because from the 780 we were able to extract a very narrow measurement of the hyperfine ^{87}Rb . Due to the limited signal to noise and the large modulation depth used, we were only able to establish the 24 kHz FM linewidth as the upper limit of our

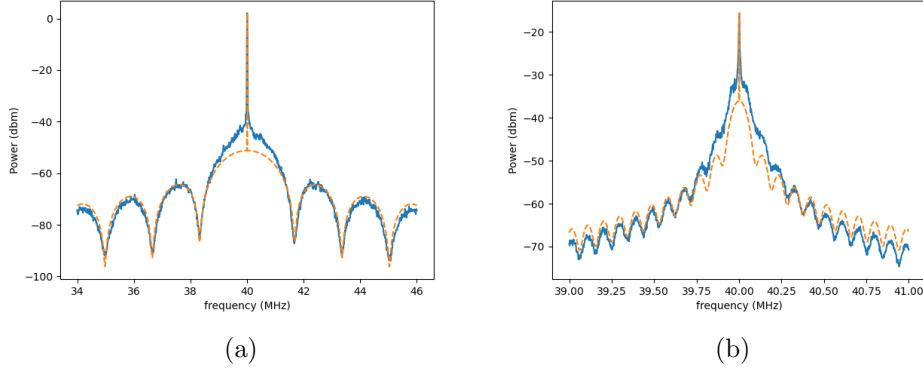


Figure 4.5: (a)PSD of the 780 nm ECDL using a 120 m Delay Fiber,(b)PSD of the 780 nm ECDL using a 2000 m Delay Fiber

780 ECDL. Thus, our expectation was to measure a value lower than that.

Using the modified PSD established in section 4.2, we fit the 780 nm data for the 125 m and 2 km fibers, as shown in figure 4.5. As can be seen, both fits show significant distortion around the center lobe. This is likely due to broadening effects such as current and fiber noise. It is likely that fiber noise is the main contributor as we would expect longer fibers to distort the spectrum more, due to the higher possibility of phase jittering, and in fact that is what is observed. Later we will discuss how fiber noise can be accounted for in the fit.

From our fits we were able to extract the linewidths from the 120 and 2000 m fibers to be 1.5 kHz and 8.8 kHz respectively. Both values agree with our assumption that we would expect a value to be lower than 24 kHz.

We assumed that the 1.5 kHz is the nearest estimate to the true linewidth due to the fact that, as established in section 3.1, the estimate of the linewidth in this sub coherent arrangement is much more sensitive to the contrast of side lobe extrema. Typically one would choose to use the 1st set of extrema as fixed points to extract the linewidth from, as I did in 3.4. This is because further points are much more susceptible to the influence of the noise floor. From Fig 4.5b, we see significant distortion of the far away extrema, but we also see the noise envelope obscuring the low order extrema. Fig 4.5a, instead shows very good agreement for the first lobe and only slight distortion for the second and third set of extrema.

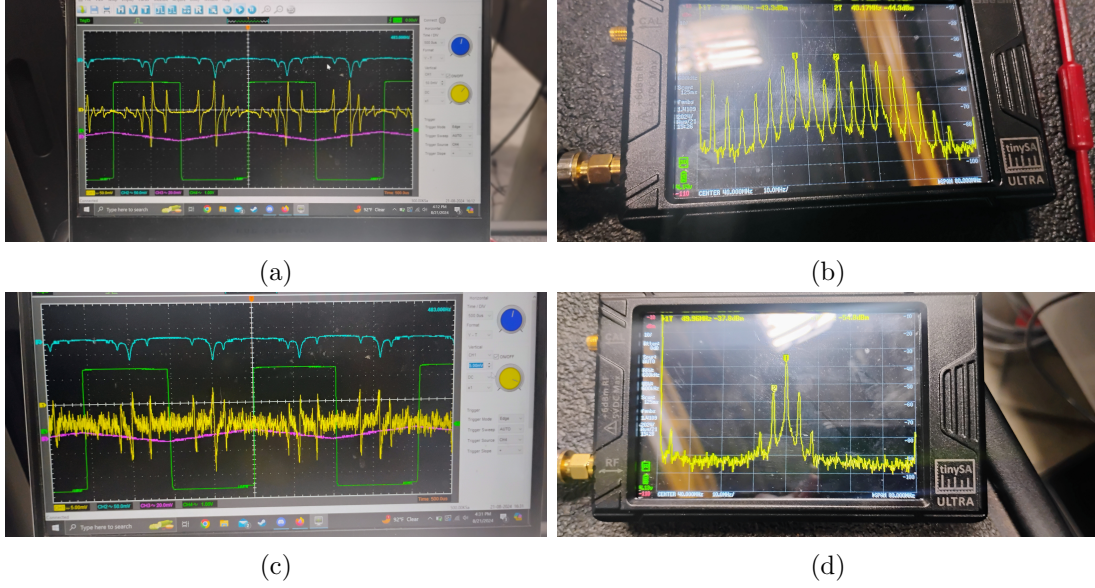


Figure 4.6: (a) ^{87}Rb Spectrum with large modulation depth, (b)PSD of 780 nm ECDL with large Modulation Depth, (c) ^{87}Rb Spectrum with small modulation depth, (d)PSD of 780 nm ECDL with Small Modulation Depth

As a demonstration as to why the 780 can not be measured in its locked state, Fig 4.6 demonstrates both the derivative signal generated by the FM dithering (a,c) and the spectrum achieved when dithered (b,d). Fig 4a clearly has the best saturated absorption spectrum, but this was done with a very large modulation depth which resulted in a multiple peaks in the PSD 4 MHz apart. Alternatively, we ran the experiment at a modulation depth near 1, and this produced a much better PSD, but the signal to noise for locking was clearly a lot worse (Fig 4.6d). The fact that the PSD has these modulation peaks in them spoils the laser linewidth as the power is distributed between multiple peaks.

Linewidth and Delay Time Results				
Delay Length (m)	Fiber	780 nm ECDL (kHz)	729 nm Toptica Laser (kHz)	950 nm DFB (kHz)
120		1.5	7.8	9.1
2000		8.8	23	1.4

Table 4.1: Linewidth of Different Lasers using 120 m and 2000 m Delay Fibers

Fig 4.7a-d further show the effectiveness of using a short delay fiber. These are scans of both the turn-key diode laser from Toptica, and our home built DFB laser. The results of these fits are summarized in table 4.1. In Fig 4.7 a and c, we can see very

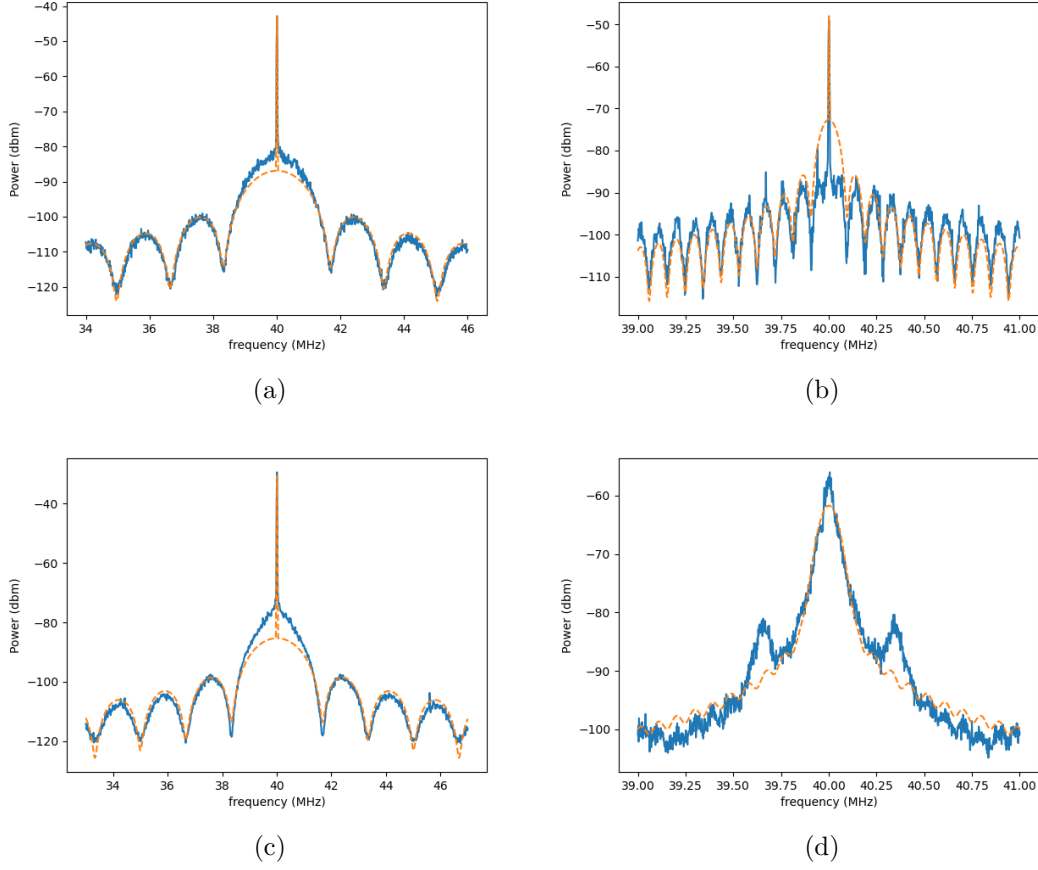


Figure 4.7: (a)950 nm DFB PSD with 120 m Delay, (b)950 nm DFB PSD with 2000 m Delay, (c)720 nm DL Pro PSD with 120 m Delay, (d)720 nm DL Pro PSD with 2000 m Delay

good agreement between our regression fit and the measured spectrum. Both PSD show regular side lobe patterns and very little excess bulding in the center lobe. Fig 4.8 b and d on the other hand demonstrate multiple issues that make them hard to fit. The 2000 m fit of 729 nm laser (Fig 4.7 d) demonstrates very small coherence peaks that makes it hard to fit to the exact PSD, but also has some broadening and anomalous features that makes Lorentzian fitting inaccurate. The DFB laser has a very inconsistent spectrum, but the side lobe contrast is much higher than would be expected. Ultimately, the loss of laser power through long delay fibers and the the introduction of fiber noise makes the use of very long fibers non ideal for linewidth extraction.

4.4 Spectrum Broadening Noise Sources

The main limiting factors in our estimation of our laser linewidths are noise sources that contribute some broadening feature to the final PSD. By definition, stochastic processes do not have closed analytic expressions because of their random nature, but the PSD often does have an analytic expression. This is how we derived the natural linewidth of the laser to be a lorentzian. This lorentzian profile comes from homogeneous noise sources, that is to say that the noise level is the same for all frequencies.

We are specifically talking about the PSD of the frequency noise, which is related to the phase noise PSD by:

$$S_\nu(f) = f^2 S_\phi(f). \quad (4.3)$$

This is to say that white noise describes both $1/f^2$ phase noise and constant frequency noise.

The most common type of inhomogeneous noise is $1/f^3$ phase noise, or $1/f$ frequency noise, often called pink noise or flicker noise. Flicker noise typically arises in our laser from power fluctuations. This type of noise also has a analytic PSD, in the form of a Gaussian.

In general, laser noise is often characterized by $1/f^\alpha$ noise sources. As these noise sources die of faster for larger order of α , it is typically required to measure for longer times to see higher order noise profiles [18, 19]. There have been studies that have been able to characterize Brownian noise $-1/f^2$ frequency noise– in DFB and DBR lasers [20], but treatment of these higher order noises are more involved and does not have a simple expression like pink or white does.

A fully rigorous treatment of the PSD would involve an expression that is the convolution of the natural Lorentzian lineshape of the laser with higher order noises [21]. This is where the Voigt profile in the incoherent DSH method arises from. Phase noise in the fiber results in power fluctuations at the detector, causing the lorentzian and gaussian noise profiles to overlap [10].

In order to demonstrate the effect of Flicker noise, we fit a single gaussian to the center

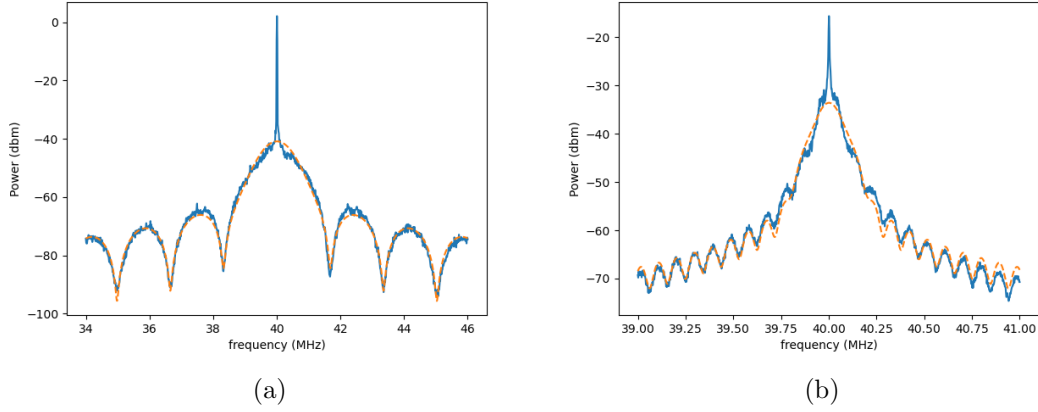


Figure 4.8: (a) Fit to 780 nm PSD using a Correction for $1/f$ Noise in 120 m Fiber, (b) Fit to 780 nm PSD using a Correction for $1/f$ Noise in 2000 m Fiber

peak as shown in Fig 4.8. These plots use the same data as the 780 nm estimate from figure 4.5. While it is not a fully rigorous fit to the constitutional model, we still improved the closeness of the fit here. For the 120 m and 2 km, we extracted new linewidths of 2.4 kHz and 10 kHz respectively.

The hope would be that fitting the entire spectrum, including broadening noises, would result in linewidth estimates converging for all fiber lengths, controlling for noise floor truncation. From figure 3.4, we already know that the contrast between adjacent extrema scales exponentially with linewidth, thus it is fair to assume that our results in section 4.3 and the results reported above agree with each other. This also confirms our assumption that even ignoring broadening features, closeness of the fit to the side lobe features and extrema is a more reliable estimate for linewidth, especially because contrast improves significantly with shorter delay times

We have reason to assume that the significant distortion in the central lobe is due to current noise. This is because we also did linewidth estimations of the 950 nm DFB with a worse current supply. The results presented in 4.3 were done with both 780 nm and 950 nm lasers running off a Vescent D2-105-200 power supply, which is regarded for its low noise operation. On the other hand, fig 4.9 shows the PSD of the DFB running of a Wavelength Electronics MPL-500 Laser Diode Driver. This driver has a significantly larger current noise ($3 \mu A$ rms [22]) compared to the the vecsent driver (50 nA rms [23]). Current noise, when sufficiently small, should only present as power fluctuations.

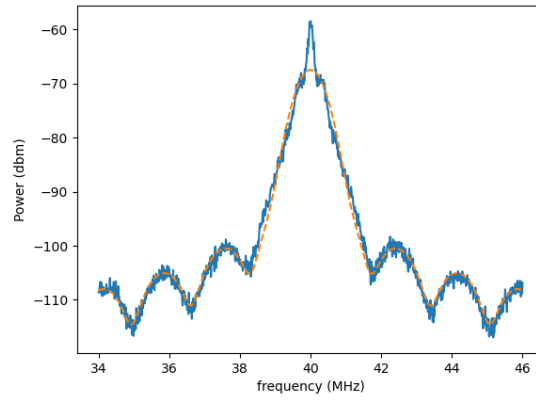


Figure 4.9: Current Induced 1/f Noise in 950 nm DFB

As discussed, this means the noise should resemble flicker noise and as such should follow a gaussian. Fig 4.9 is a fit to the data including a gaussian to the center lobe.

5 Conclusion

The technique demonstrated in this paper, where a delay fiber shorter than the coherence length of a light source, has been shown to produce linewidth estimations of better quality than traditional means. We have demonstrated that fibers short enough to produce well resolved coherence in the PSD can allow one to determine laser linewidths while reducing external fractional noise that distorts the PSD of lone delay fibers. We also demonstrated a technique to extract the linewidth from data that demonstrated prominent $1/f$ noise.

References

- [1] Warren G. Nagourney. *Quantum Electronics for Atomic Physics*. Oxford University Press, 2010.
- [2] Roy M. Howard. *Principles of Random Signal Analysis and Low Noise Design*. John Wiley Sons Inc., 2002.
- [3] Dutta Nilloy K. Agrwal, Govind P. *Semiconductor Lasers*. ATT, 1993.
- [4] Lax M. Classical noise. v. noise in self-sustained oscillators. *Physics Review*, 160(290), 1967.
- [5] J. P. Gordon, H. J. Zeiger, and C. H. Townes. The maser—new type of microwave amplifier, frequency standard, and spectrometer. *Phys. Rev.*, 99:1264–1274, Aug 1955.
- [6] Inc. Thorlabs. Fabry-perot interferometer tutorial.
- [7] Zhongan Zhao, Zhenxu Bai, Duo Jin, Xiaojing Chen, Yaoyao Qi, Jie Ding, Bingzheng Yan, Yulei Wang, Zhiwei Lu, and Richard P. Mildren. The influence of noise floor on the measurement of laser linewidth using short-delay-length self-heterodyne/homodyne techniques. *Micromachines*, 13(8), 2022.
- [8] L. Richter, H. Mandelberg, M. Kruger, and P. McGrath. Linewidth determination from self-heterodyne measurements with subcoherence delay times. *IEEE Journal of Quantum Electronics*, 22(11):2070–2074, 1986.
- [9] Zhongan Zhao, Zhenxu Bai, Duo Jin, Yaoyao Qi, Jie Ding, Bingzheng Yan, Yulei Wang, Zhiwei Lu, and Richard P. Mildren. Narrow laser-linewidth measurement using short delay self-heterodyne interferometry. *Opt. Express*, 30(17):30600–30610, Aug 2022.
- [10] Mo Chen, Zhou Meng, Jianfei Wang, and Wei Chen. Ultra-narrow linewidth measurement based on voigt profile fitting. *Opt. Express*, 23(5):6803–6808, Mar 2015.

- [11] Shihong Huang, Tao Zhu, Zhenzhou Cao, Min Liu, Ming Deng, Jianguo Liu, and Xiong Li. Laser linewidth measurement based on amplitude difference comparison of coherent envelope. *IEEE Photonics Technology Letters*, 28(7):759–762, 2016.
- [12] Thorlabs. Diffraction grating tutorial. https://www.thorlabs.com/newgrouppage9.cfm?objectgroup_id=9026.
- [13] L.B. Mercer. $1/f$ frequency noise effects on self-heterodyne linewidth measurements. *Journal of Lightwave Technology*, 9(4):485–493, 1991.
- [14] Daniel A. Steck. ‘rubidium 87 d line data. <https://steck.us/alkalidata>.
- [15] P Rupasinghe, Fiona Wee, Thomas Bullock, and Jiaxing Liu. Measurement of hyperfine constants and the isotope shift of rubidium 5p $1/2$ excited-state using saturated absorption spectroscopy. *Physica Scripta*, 98, 03 2023.
- [16] C. C. Kwong, E. A. Chan, S. A. Aljunid, R. Shakhmuratov, and D. Wilkowski. Large optical depth frequency modulation spectroscopy. *Opt. Express*, 27(22):32323–32336, Oct 2019.
- [17] P. Welch. The use of fast fourier transform for the estimation of power spectra: A method based on time averaging over short, modified periodograms. *IEEE Transactions on Audio and Electroacoustics*, 15(2):70–73, 1967.
- [18] Bruno Fermigier and Michel Tetu. Frequency noise, Allan variance, and lineshape of semiconductor lasers. In Pierre Galarneau, editor, *Laser Diodes and Applications III*, volume 3415 of *Society of Photo-Optical Instrumentation Engineers (SPIE) Conference Series*, pages 164–172, October 1998.
- [19] Stefano Camatel and Valter Ferrero. Narrow linewidth cw laser phase noise characterization methods for coherent transmission system applications. *Journal of Lightwave Technology*, 26(17):3048–3055, 2008.

- [20] E. Uruñuela, M. Ammenwerth, P. Malik, L. Ahlheit, H. Pfeifer, W. Alt, and D. Meschede. Raman imaging of atoms inside a high-bandwidth cavity. *Phys. Rev. A*, 105:043321, Apr 2022.
- [21] Weichao Ma, Bing Xiong, Changzheng Sun, Xu Ke, Zhibiao Hao, Lai Wang, Jian Wang, Yanjun Han, Hongtao Li, and Yi Luo. Laser frequency noise characterization by self-heterodyne with both long and short delay. *Appl. Opt.*, 58(13):3555–3563, May 2019.
- [22] Wavelength Electronics Inc. Mpl500 500ma laser diode driver. <https://www.teamwavelength.com/product/mpl500-laser-diode-driver/?srsltid=AfmBOooKhFBpJZtqo9zZdrIOjh-GAYI-P3ly8D-owsmS7MMD2kOhdQIJ>.
- [23] Vescent Photonics Inc. D2 laser controller. <https://vescent.com/products/66e9e0500e744f31ce5ee11f>.

Curriculum Vitae

Genevieve Gutierrez

4505 S Maryland Pkwy, Las Vegas, NV 89154

gengutierrez702@gmail.com

Work Experience

Graduate Researcher, 2023 - Present

University of Nevada, Las Vegas

Master Thesis Project: sub-coherent characterization of ultrastable laser lineshapes.

This includes in depth knowledge of random signal analysis and non-linear fittings

Under the guidance of Dr. Yan Zhou, I work on computer aided simulations of ion trap dynamics, assist in vacuum chamber design and maintenance, and build optics experiments

Designed system for frequency modulated spectroscopy for the purpose of ultrastable laser locking and control

Graduate Teaching Assistant, 2023-May 2025

University of Nevada, Las Vegas

Lead hands on laboratory class on topics of mechanics, electronics, optics and fluid mechanics

Instructed students on various levels of understanding with the goal of meeting them where they are and getting them to grasp the greater physics concepts

UNLV Internships, 2022 - 2023

University of Nevada, Las Vegas

NSF EPSCor Undergraduate Research Fellowship

UNLV OUR Undergraduate Research Fellowship

Trapping and Cooling for Ca^+ for Cold Ion-Radical Collisions under Dr. Yan Zhou's lab

Publications

Li, J., Fernandez, R., **Gutierrez, B.**, Pedersen, J., and Zhou, Y. (2024). Advancing Molecular Spectroscopy Efficiency with Extensive Parallelism. Metrology, 4(4), 736–764. <https://doi.org/10.3390/metrology4040043>

Li, J., Mcpartland, T., **Gutierrez, B.**, Pedersen, J., and Zhou, Y. (2023). Additive manufacturing for ultra-high vacuum components: Leveraging photo-polymer resin technologies. Vacuum, 220, 112769–112769.
<https://doi.org/10.1016/j.vacuum.2023.112769>

Education

M.A. in Applied Physics; Atomic, Molecular and Optical Physics University of Nevada, Las Vegas August 2025

B.A. in Applied Physics and Mechanical Engineering University of Nevada, Las Vegas May 2023

Skills

Computer Languages

Python

MATLAB

Mathematica

CAD

Solid Works

COMSOL